# CRYSTAL GROWTH & DESIGN

Continuous-Flow Sonocrystallization in Droplet-Based Microfluidics

Damiano Rossi,[†] Rashid Jamshidi,[†] Nader Saffari,[‡] Simon Kuhn,[§] Asterios Gavriilidis,[†] and Luca Mazzei*,[†]

[†]Department of Chemical Engineering and [‡]Department of Mechanical Engineering, University College London, Torrington Place, London WC1E 7JE, U.K.

[§]Department of Chemical Engineering, KU Leuven, W. de Croylaan 46, 3001 Leuven, Belgium

ABSTRACT: A novel design for continuous flow sonocrystallization of adipic acid in a capillary device is presented and investigated experimentally and numerically. The effect of supersaturation and ultrasound power is studied. To elucidate the relationship between crystallization and cavitation, sonochemiluminescence and sonoemulsification experiments are performed, and numerical investigation of the wave propagation in aqueous solution is used to predict the probability of cavitation. Crystal size distribution at different operating conditions is obtained by laser diffraction. Narrow size distributions, small mean size of crystals (ca. 15 μm), and high crystal production rate are achieved when applying ultrasound. In addition, numerical simulations of pressure distribution show that high pressure amplitudes are obtainable near the vicinity of the sonoprobe tip. Using a cavitation threshold formulation, the distance from the tip where transient cavitation takes place is quantified. The results are in agreement with the experimental findings, in which by increasing the distance between capillary and sonoprobe, emulsification, sonochemiluminescence, and nucleation decrease. It is concluded that transient cavitation of bubbles is a significant mechanism for enhancing nucleation of crystals among the several proposed in the literature.

300 μm
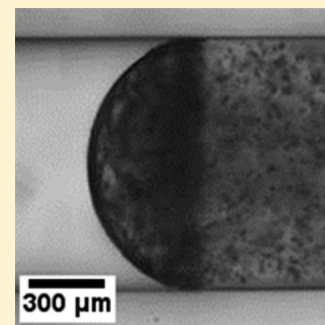
1. INTRODUCTION

Reproducible and narrow crystal size distributions (CSDs), as well as small mean crystal sizes, are desirable characteristics in the production of crystalline materials. These targets are particularly desirable in the pharmaceutical industry for obtaining homogeneous physical crystal properties, and in turn enhancing drugs bioavailability, and for simplifying crystal slurry separation and particulate tableting.[1]

Presently, pharmaceuticals are normally produced in batch or semicontinuous operation using standard stirred tank crystallizers. In industry, batch processes are usually preferred to continuous processes, since the former show less encrustation issues. However, continuous crystallization is an attractive solution because of the smaller volumes required, the lower operating and labor costs, and the greater product reproducibility.[2] In batch systems, process parameters such as temperature and concentration—crucial in cooling-driven crystallization—may not be uniform. This hinders batch to batch reproducibility. One of the most undesired consequences of the heterogeneous distribution of temperature and concentration within the reactor is the broad size distribution of the crystals.[2] For this reason, recently there has been an increased interest in the development of novel crystallization methods. In this regard, microfluidic devices offer great potential in delivering chemical compounds of higher quality. The benefits that they present have been widely reported in the literature:[3,4] milli and micro characteristic lengths lead to greater surface-to-volume ratios, intensifying mass and heat transfer, reducing temperature and concentration nonuniformities, and providing greater efficiency and control than those achievable in large reactors. As a result, in the last two decades microreactor engineering has become an area of increasing interest for researchers, in particular, for the screening of proteins,[5] and for industry, for instance, for producing nanoparticles.[6] In spite of the benefits just mentioned, the application of microchannels still requires high fabrication costs. In addition, once a microchip has been manufactured, there is rarely any opportunity to alter the device. Finally, these reactors are not well suited to handling solids, clogging representing a major hurdle when particles are in the same size range as the channel.[4] Nowadays, the most attractive successful anticlogging technique involves performing crystallization in droplets that travel through the microchannel inside a carrier phase (liquid/liquid two-phase). By using disperse-phase droplets as individual reactors, it is possible to confine the solid product inside the droplets, thereby keeping it away from the walls of the channel, avoiding its occlusion.[7]

Owing to the stochastic nature of crystal nucleation and the strong dependence of nucleation rate on supersaturation, to further increase process control and reproducibility, seeding has been used in large batch and continuous crystallization processes[2] and recently also in milli-tubular flow-through devices.[8,9] Intentional seeding is a common technique used in industrial processes for controlling the CSD by inducing nucleation on demand and shortening the induction times. Unfortunately, such technique requires operator intervention as well as additional engineering for monitoring the seed addition. Postcrystallization micronization techniques (for instance, milling, crushing, and grinding) are an alternative for controlling the CSD but are generally expensive and may adversely affect the product properties.[2]
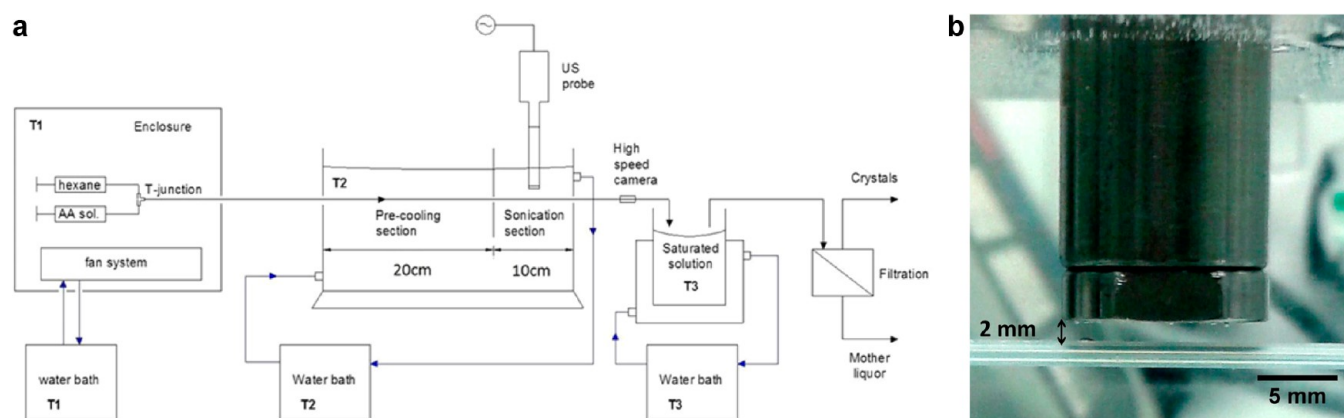
Figure 1. Experimental setup: (a) schematic of the droplet-based capillary sonocrystallizer, (b) horizontal alignment between the sonoprobe tip and the capillary.

Sonication, that is, the application of power ultrasound to process fluids, is an intensification technology that, when applied to crystallization, permits improving and tailoring both process and product quality. Cavitation occurring during the ultrasonic irradiation is commonly regarded as the principal mechanism that promotes crystal nucleation.[10−12] The link between the two phenomena, however, is still a subject of research, and various mechanisms have been recently proposed.[13−15] The use of ultrasound offers a method to drastically reduce the induction time and supersaturation required to induce nucleation and to narrow the CSD.[16] Furthermore, it modifies the crystal habit, increasing crystal purity and reproducibility.[16−21] The main advantage that sonication offers is that seeding is no longer needed to induce primary nucleation, because acoustic cavitation attains the same result more effectively and with better control. This is particularly welcome in pharmaceutical processes. Ultrasound generators operate remotely and therefore are suitable for contained, sterile environments. Issues such as seeds choice and contamination are eliminated.[22] Moreover, the supersaturation level where nucleation should be induced can be easily controlled at the flick of a switch. For these reasons ultrasound technology has received significant impetus recently, partly in response to the increased demand for complex chemicals that must comply with exacting standards and to the need for environmentally clean processing and inexpensive equipment.[16,17] The use of ultrasound is also expected to overcome problems associated with channel clogging and the pumping of suspensions. This has been demonstrated for the flow of particle suspensions in microchannel heat exchangers, where fouling was drastically reduced in the presence of ultrasound.[23−26]

In this work, we seek to obtain better control of crystal size by running for the first time cooling crystallization in a compact experimental setup that combines continuous flow in microchannels and ultrasound technologies. Cooling crystallization of adipic acid from aqueous solution was the selected case study, and hexane, used as carrier fluid, was employed to generate the segmented flow pattern required to overcome the clogging issue. The effects of supersaturation and ultrasonic power in a confined tubular geometry on crystal size, crystal size distribution, and crystal production were investigated. To this end, a filtration protocol was developed for separating hexane and water from the crystals formed in the droplets. The designed droplet-based capillary sonocrystallizer is suitable for

studying the effects of specific sonication conditions on crystallization, because of the flexibility that our setup offers to adjust the distance between the ultrasonic source and the small portion of the sonicated solution, in contrast to fixed geometries where the sonication conditions are not adjustable.[27] The specific pressure field inside the capillary was calculated by means of numerical simulation. This allowed estimating the possibility of cavitation and relating it to sonocrystallization. Moreover, evidence of cavitation was also provided by observing the occurrence of sonoemulsification[28] and by detecting the presence of sonochemiluminescence.[29]

2. EXPERIMENTAL SECTION

2.1. Chemicals. Adipic acid (hexanedioic acid, $(CH_2)_4(COOH)_2$, >99.5% pure, Sigma-Aldrich, UK) was used as received without further purification, and solutions were made in deionized water (conductivity < 0.2 μS/cm). The solubility of adipic acid in water at different temperatures was determined by fitting experimental data reported in the literature.[2] n-Hexane $((CH_3)(CH_2)_4CH_3 > 97\%$ pure, max. 0.005% water, VHR, UK) was used as received, without further purification, and was the selected carrier fluid for generating the segmented flow.

2.2. Experimental Setup and Procedure. Figure 1a shows the schematic of the droplet-based capillary sonocrystallizer used in this work. The segmented flow was successfully employed in previous work to prevent clogging in a hydrophobic tubular geometry.[30] The two-phase flow was obtained with PFA capillaries (ID = 1 mm, OD = 1.5 mm) connected to two Harvard PHD 2000 syringe pumps followed by polychlorotrifluoroethene (PCTFE) filters (average pore size: 2 μm) and a PEEK T-junction (ID = 0.5 mm). The pumps and T-junction were located inside a temperature-controlled Perspex enclosure in which the adipic acid solution was kept undersaturated at temperature T_1 = 30 °C. The temperature inside the Perspex enclosure was maintained constant by a fan heater. Flow rates of 0.3925 mL/min were used for both fluids.

According to the thermal path illustrated in Figure 2, the droplets move from temperature T_1 to temperature T_2 to reach a specific supersaturation. The initial adipic acid concentration is 2.12 g per 100 g of water, which is the saturation concentration at room temperature (22 °C). Six cooling temperatures were employed, T_2 = 6 °C, 8 °C, 10 °C, 12 °C, 14 and 16 °C, corresponding to supersaturations of S = 2.62, S = 2.39, S = 2.12, S = 1.86, S = 1.63 and S = 1.42, respectively.

The capillary was horizontally aligned within a Perspex container (L = $L_1 + L_2$ = 30 cm, W = 20 cm, H = 25 cm). To keep the capillary perfectly horizontal, two threads were made in the center of the lateral walls of the container, and the capillary was tightened between two opposite IDEX nuts (Figure 1a). The Perspex container was divided in two communicating chambers and filled up with cooling water at T_2 which recirculated through a second water bath. The first chamber had a length L_1 = 20 cm and worked as a precooling section. The length L_1
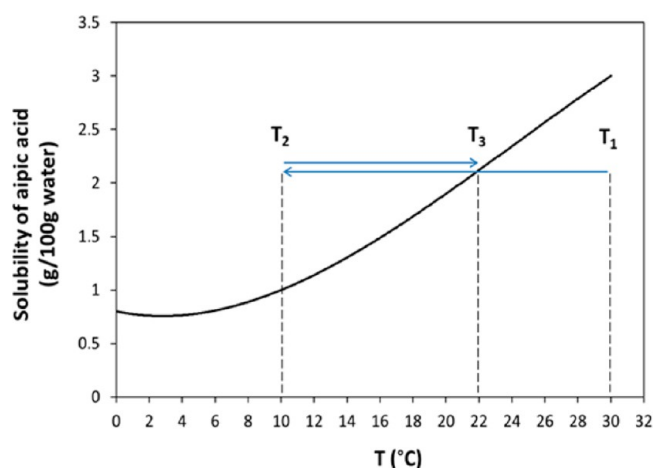
Figure 2. Temperature profile in the various stages of the droplet capillary sonocrystallizer.

was fixed taking into account the temperature profiles along the capillary which were calculated using numerical simulation and are plotted in Figure 3 for the simplified single-phase water system. The
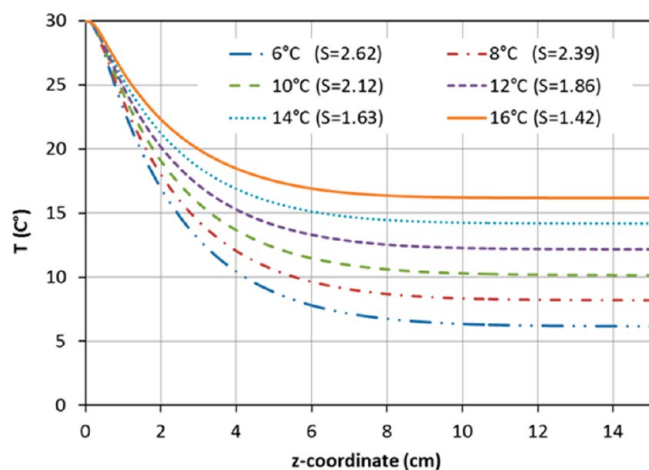
Figure 3. Temperature profile along the capillary axis obtained numerically at different cooling temperatures: from 30 to 6 °C (S = 2.62), 8 °C (S = 2.39), 10 °C (S = 2.12), 12 °C (S = 1.86), 14 °C (S = 1.63), and 16 °C (S = 1.42).

simulations were conducted using COMSOL Multiphysics. As can be observed from the profiles, a plateau in temperature was achieved after about 15 cm from the inlet of the precooling section. That is why we decided to place the sonoprobe at the distance $L_1 + (L_2/2) = 25$ cm from the section inlet. The effective achievement of the desired temperature T_2 was checked using a thin thermocouple placed within the capillary by means of a PEEK T-junction (ID = 1 mm).

Ultrasound was applied by fixing an ultrasonic probe (Cole-Parmer Instruments 750 W ultrasonic processor, frequency = 20 kHz and amplitude = 21%) after the precooling section in the middle of the sonication section (of length $L_2 = 10$ cm). The center of the 13 mm circular flat sonoprobe tip was horizontally aligned to the capillary using an adjustable stage holder that allowed us to clamp the sonoprobe, controlling and setting different distances between the sonoprobe tip and the capillary external wall. Experiments were initially run with a tip-capillary external-wall distance of 2 mm (Figure 1b). Each droplet experienced a residence time of less than 1 s below the sonoprobe and a total residence time of 18 s within the Perspex container.

2.3. Crystal Detection and Filtration Protocol. Crystallization was detected by placing a high-speed camera (Fastcam MC1 Photron)

attached to an optical microscope (Olympus IX50) immediately after the sonoprobe (Figure 1a). To improve crystal detection and eliminate light reflection problems owing to the curvature of the lateral walls of the capillary, we used a refractive index matching device in the microscope unit. The capillary was immersed in a plastic box filled with water at room temperature (22 °C) and fixed by guides that allowed moving the capillary in front of the microscope lens. Because of the small dimensions of the box, the crystals experience a very short residence time (around 1 s); hence, no significant crystal growth can occur. Accordingly, we can safely assume that the CSD is not affected in the refractive index matching device.

A filtration protocol was developed to separate the crystals from the mother liquor droplets to determine their CSD. Hexane and water droplets with crystals were collected in a 50 mL saturated solution kept at $T_3 = 22$ °C (Figure 2). The collection time was set so that the solute concentration in the resulting solution remained virtually unchanged (a 5% maximum decrease was accepted). This condition ensured that no significant crystal shrinkage or dissolution occurred in the collected mother liquor (nucleation and growth cannot take place because the solution is not supersaturated), so that during the collection time the crystal size distribution was not altered. The collection time was set to 10 min. Even in the situation in which ultrasound consumes the total available solute at the lowest temperature T_2 considered (making the solute reach its lowest concentration in the stream leaving the sonication section), a collection time of 10 min was found to meet the requirement given above. This was verified by solving a mass balance.

The solution containing the suspended crystals was first separated from the hexane (the two are immiscible) and then filtered by means of vacuum filtration using 0.3 μm Whatman cellulose nitrate membranes. To recover all crystalline material, the beaker and the filter funnel were washed with the prepared saturated solution of adipic acid at 22 °C. The filters were dried for 10 min on a hot plate at 80 °C and weighed to determine the mass of the crystals produced. The crystals were subsequently suspended in vegetable oil, in which adipic acid is insoluble, and homogeneously dispersed using an ultrasonic water bath for 10 min.[31] This slurry was used to determine the CSD with a laser diffraction particle size analyzer (LS 13320 Beckman Coulter).

To establish whether or not primary particles break up in the ultrasonic water bath, we compared the CSD of the raw adipic acid material (raw particles purchased, which do not present agglomerates) with that of the same crystals suspended and treated in the ultrasonic water bath for 10 min according to our protocol. Finding the two CSDs nearly identical, we concluded that in the deagglomeration stage the primary particles do not break up. This stage affects only the agglomerates.

2.4. Sonochemiluminescence. Sonochemiluminescence (SCL) refers to the light that is emitted when luminol (5-amino-2,3-dihydro-1,4-phthalazinedione) reacts with OH· radicals owing to the presence of collapsing (that is, cavitation) bubbles. The nearly adiabatic collapse of the bubbles results in the rapid generation of high temperatures and pressures as well as highly reactive OH· radicals. Luminol reacts with these radicals to produce a characteristic bluish light which is employed to map the spatial distribution of active cavitation bubbles.[32] This technique, which was traditionally used in large geometries, has been recently adopted to demonstrate the cavitation activity in small geometries and microreactors.[29,33,34]

In this work, SCL experiments were carried out using a deionized water solution containing 2 mM luminol (Merck) at pH = 12.[29] Luminol solution was flowed within the capillary sonocrystallizer to display the cavitation activity inside the capillary channel. To visualize the cavitation activity in the vicinity of the sonoprobe tip, the same luminol solution was also employed to fill up the Perspex enclosure. Images were captured in a dark room using a Nikon D60 camera with an 18−55 mm lens at a 35 mm focal distance. The exposure time was 3 min, the focal ratio was 5.0, and the ISO setting was Hi1.[35]

3. NUMERICAL SIMULATION OF ULTRASOUND WAVE PROPAGATION IN THE PERSPEX ENCLOSURE

To elucidate the correspondence between transient cavitation and enhancement of crystallization in the current sonocrystallizer, we simulated the wave propagation in the liquid inside the temperature-controlled Perspex enclosure containing the capillary. The idea was to shed light on how acoustic waves, and the consequences of their propagation in water such as transient cavitation, can possibly influence nucleation of crystals. To this end, a linearized model, which is accepted to give reasonable results for pressure amplitudes and which accounts for wave attenuation owing to presence of bubbles, was solved using the finite element method.

Commander and Prosperetti[36] derived an equation for wave propagation in a bubbly liquid that considers a term accounting for the damping effect of bubbles. In this model, the modified wave equation in the frequency domain, which basically is a Helmholtz equation, reads:

$$\nabla^2 \hat{p}_a + k_m^2 \hat{p}_a = 0 \tag{1}$$

where $\hat{p}_a$ is the pressure amplitude and k_m is the complex wavenumber. For a monodispersed bubble distribution with equal equilibrium radius R_0, the complex wavenumber is

$$k_m^2 = \frac{\omega^2}{c^2}\left(1 + \frac{4\pi c^2 n_b R_0}{\omega_0^2 - \omega^2 + 2ib\omega}\right) \tag{2}$$

where c is the speed of sound in the medium, n_b is the number of bubbles per unit volume, ω is the frequency of the wave, and ω_0 is the resonance frequency of the bubbles, which is given by

$$\omega_0^2 = \frac{p_0}{\rho R_0^2}\left[\mathrm{Re}(\Phi) - \frac{2\sigma}{R_0 p_0}\right] \tag{3}$$

In this equation, p_0 is the undisturbed pressure inside the bubble, which is higher than the equilibrium pressure p_∞ in the liquid by the amount $2\sigma/R_0$ because of the surface tension σ, and ρ is the density of the medium. The complex dimensionless parameter Φ is defined as

$$\Phi = \frac{3\gamma}{1 - 3(\gamma - 1)i\chi[(i/\chi)^{1/2}\coth(i/\chi)^{1/2} - 1]} \tag{4}$$

where γ is the ratio of the specific heat capacities of the gas inside the bubble and χ is a dimensionless parameter defined as

$$\chi = \frac{D}{\omega R_0^2} \tag{5}$$

where D is the thermal diffusivity of the gas inside the bubble. The damping factor b in eq 2 is given by

$$b = \frac{\mu}{\rho R_0^2} + \frac{p_0}{2\rho\omega R_0^2}\mathrm{Im}(\Phi) + \frac{\omega^2 R_0}{2c} \tag{6}$$

in which μ is the dynamic viscosity of the medium.

In experiments, neither the initial size of the bubbles nor their quantity is straightforward to measure. However, the parameter β, which is the void fraction of bubbles, is measurable with certain techniques.[37,38] This parameter is related to n_b by

$$\beta = \frac{4\pi}{3}R_0^3 n_b \tag{7}$$

In the simulation, it was assumed that the bubbles are spatially distributed homogeneously in the medium. Typical values of $\beta = 3 \times 10^{-4}$ and $R_0 = 30$ μm were selected for the void fraction and initial bubble nuclei size.[36,39,37] The value of n_b required for eq 2 is then calculated from eq 7.

The walls of the enclosure were made of Perspex and were assumed to be pressure release boundaries. Therefore, they were modeled by a Dirichlet-type boundary condition with $\hat{p}_a = 0$ in the numerical solution of the Helmholtz equation. The frequency of the ultrasound was 20 kHz, and so the thickness of the Perspex walls was negligible with respect to the wavelength of the ultrasound wave; this justified neglecting the thickness of the Perspex walls in the simulation and adopting the Dirichlet-type boundary condition.[40] The lateral walls of the sonoprobe were considered as rigid reflecting walls (Neumann boundary condition, i.e., $\partial \hat{p}_a/\partial n = 0$). The source of ultrasound was a horn, which was also modeled using a Dirichlet-type boundary condition with $\hat{p}_a = \hat{p}_a^0$. To calculate the value of the pressure amplitude at this boundary, we could use either the plane wave formulation or the radiation from a piston radiator into a half-space, which is more precise. The plane wave formulation relates the pressure amplitude at the source boundary to the ultrasonic power transferred to the liquid; in its simplest form, it reads:[41]

$$\hat{p}_a^0 = \sqrt{\frac{2\rho c P_{US}}{S}} \tag{8}$$

in which P_{US} is the power of the ultrasound source and S is the area of the sonoprobe. To calculate the amplitude from eq 8, one should measure the power transferred to the liquid, and therefore, we used calorimetric measurements. A volume of 20 mL of deionized water was selected as the sample and fully insulated from the environment using thick layers of wool and aluminum foil. Thus, the dissipated power due to ultrasound could be evaluated by measuring the change in the temperature of the medium and accordingly the dissipated heat as

$$P_{US} = mc_p\frac{dT}{dt} \tag{9}$$

in which m is the mass of the water (20 g) and c_p is its specific heat capacity (4186 J/kg K).

The variation of temperature over time in the small beaker is shown in Figure 4. According to this temperature gradient, the
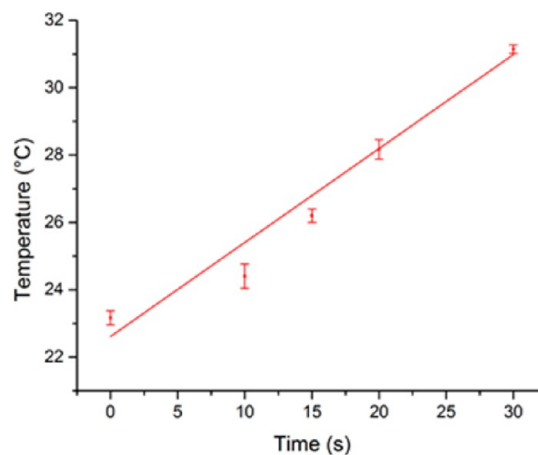
Figure 4. Temperature rise in the medium due to the dissipated power.

Table 1. Physical Properties Required for the Numerical Simulation

γ	D (m²/s)	σ (N/m)	ρ (kg/m³)	μ (Pa·s)	c (m/s)	p_0 (Pa)
1.4	1.9×10^{-5}	0.0725	1000	0.001	1480	101325

power dissipated in the medium was calculated as 8.3 W. This value was used to estimate the pressure amplitude at the tip of the sonoprobe (eq 8), which resulted in a value of 4.3×10^5 Pa. It is worth mentioning that the piston radiator model predicts a value for the pressure amplitude on the surface of the sonoprobe similar to the plane wave formulation (relative difference of 7%). However, the simpler plane wave formulation is selected here, and it provides a reasonable approximation.

The remaining physical properties required for the simulation are shown in Table 1.

Equations 1−8 were employed in a 3D simulation using COMSOL Multiphysics 4.4 in which unstructured linear-order tetrahedral elements were used. To avoid pollution effects,[42,43] the size of the elements was selected so that the following rule was satisfied for the simulation:

$$k \cdot h \ll 1 \tag{10}$$

in which k is the wavenumber, equal to ω/c, and h is the average size of the edges of the elements. To carry the grid independency study, different sizes for the edges were selected. Finally, a grid with 504895 degrees of freedom (DOF) containing 366124 tetrahedral elements was used. For this quantity of DOFs, it is possible to solve the Helmholtz equation using one of the direct solvers available in the software. Thus, the MUMPS (Multifrontal Massively Parallel Sparse direct Solver) was implemented to solve the equation on a machine with a 64-bit windows operating system and Intel Core i5-3470 CPU at 3.2 GHz speed and 8.0 GB RAM. The required time for the simulation was approximately 1 h.

Lastly, we investigated the space dependent probability of transient cavitation by knowing the pressure amplitude along the axis of the sonoprobe, computed from the 3D simulation. Several thresholds for the minimum pressure amplitude required for transient cavitation of bubbles are available in the literature. Here, we selected a globally accepted threshold which is suggested by Lauterborn.[44] According to this criterion, if the shrinkage velocity of the bubble wall (dR/dt) exceeds the speed of sound at the time of collapse, the bubble undergoes violent collapse and the cavitation is categorized as transient. Therefore, one should solve a Rayleigh-Plesset type equation for the radial dynamics of the bubbles. Here, the dynamics of the bubbles, including the compressibility effects of the surrounding liquid to the first order of the acoustical Mach number ($Ma = \dot{R}/c$), was modeled by means of the Keller-Miksis equation:[45]

$$\rho\left[\left(1 - \frac{\dot{R}}{c}\right)R\ddot{R} + \frac{3}{2}\left(1 - \frac{\dot{R}}{3c}\right)\dot{R}^2\right]$$
$$= \left(1 + \frac{\dot{R}}{c} + \frac{R}{c}\frac{d}{dt}\right)\left(p_g - \frac{2\sigma}{R} - \frac{4\mu\dot{R}}{R} - p\right) \tag{11}$$

in which overdots stand for differentiation with respect to time and p is the pressure in the liquid at the bubble center in the presence of a sound field $p = p_0 - \hat{p}_a \sin(\omega t)$. To solve this equation, we assumed an initial bubble size of $R_0 = 30 \ \mu$m.[37] Moreover, the amplitude of the acoustic pressure, $\hat{p}_a$, was calculated from the numerical simulation. Using this analysis,

we predict regions inside the Perspex box, and more specifically along the axis of the sonoprobe, in which we expect transient cavitation. Thus, we can illustrate how the experimental observations such as sonochemiluminescence and enhancement of nucleation are related to the consequences of transient cavitation.

4. RESULTS AND DISCUSSION

4.1. Crystal Size Distribution and Crystal Production. To check the reproducibility of the experiments performed with the designed sonocrystallizer, each experiment was repeated three times and the CSD was measured. As a slight scattering in the CSD results was observed for each of the six supersaturations investigated, for each case we report the average result based on the three experimental values found. The corresponding representative error bars are reported at the peak of each curve (Figure 5). The data variability is attributed to the
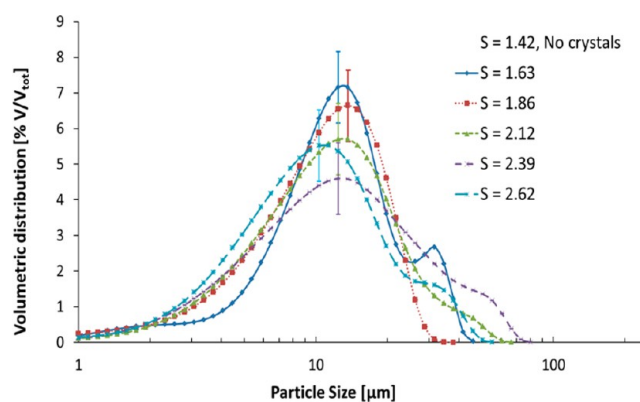

Figure 5. Effect of supersaturation on CSD. Supersaturations investigated: S = 2.62, 2.39, 2.12, 1.86, 1.63, and 1.42. Hexane and adipic acid solution flow rates = 0.3925 mL/min. Sonoprobe tip - capillary external wall distance = 2 mm. Ultrasonic system: Cole-Parmer Instruments 750 W ultrasonic processor, frequency = 20 kHz and amplitude = 21%.

experimental error as well as to the crystal separation process, which involves a series of additional operations that cannot be perfectly controlled and monitored. Because the CSD curves were not obtained by a nonintrusive online crystal detection method, data variability induced by the complex filtration protocol has to be considered as part of the overall experimental error. The results shown make us conclude that the supersaturation level does not have a remarkable effect on the CSD, and in turn on the resulting mean crystal size. The curves in Figure 5 have similar shapes, and, as one can see, overlap within the experimental error bars. A practically constant mean size $D_{4,3}$ value was measured and found to be around 15 μm for all the supersaturations investigated. The $D_{4,3}$ mean size provided by the laser diffraction measurements is defined as the ratio between the fourth and third moments (m_4 and m_3) of the crystal size distribution $n(L)$; consequently, it is

$$D_{4,3} \equiv \frac{m_4}{m_3} \equiv \frac{\int_0^\infty L^4 n(L)\, dL}{\int_0^\infty L^3 n(L)\, dL} \qquad (12)$$

Even if the optical properties of the vegetable oil used did not allow us to clearly distinguish the crystal morphologies, by checking several snapshots (two are shown in Figure 6) we
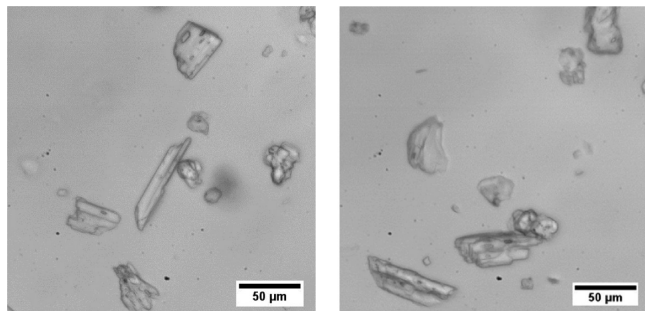
Figure 6. Two different pictures of adipic acid crystals after the deagglomeration step in vegetable oil.

believe that the higher mode in the CSDs reported in Figure 5 is predominantly due to large primary particles. These particles form within the capillary sonocrystallizer under the conditions described in the Experimental Section, giving the CSDs reported in Figure 5.

Narducci et al.[46,47] designed an MSMPR continuous sonocrystallization process able to produce adipic acid crystals with the same sonication system employed in this article. However, because of the large volume of the system, this could not work with small residence times, and consequently crystal growth played a significant role during the crystallization process. As a result, a quite larger mean crystal size (>30 μm) was observed as compared with our case. On the other hand, the microscale geometry employed here allows performing experiments with very small residence times (less than 1 s). Crystal nucleation significantly occurred during such short times when ultrasound was applied. Crystals were collected immediately after the sonication stage; no growth section was present in the setup. This shows how quick the sononucleation process is. As soon as the desired supersaturation was reached, we immediately got crystals when the sonoprobe was switched on, whereas no crystals were visible when the sonoprobe was switched off. Crystals were created at all the supersaturations investigated except for S = 1.42 (Figure 9b). This value represents a sort of threshold below which the application of ultrasound does not have any effect, and therefore crystals do not form, as in silent conditions (Figure 9h). In conclusion, the capillary sonocrystallizer represents a promising solution for obtaining very small crystals with a reproducible mean size in a very short time. The apparatus leads to crystals one order of magnitude smaller than the commercial adipic acid raw material from suppliers, micronized materials, and hammer milled materials.[47]

Assuming no crystal loss during washing, and neglecting the amount of retained mother liquor and impurities, the crystal yield Y is calculated as

$$Y(\%) = \frac{\Delta m_{filt}}{\Delta m_{eq}(T_2)} \times 100 \qquad (13)$$

Y represents the percentage of the mass of adipic acid crystallized and therefore filtered (Δm_{filt}) over of the maximum mass that theoretically can be crystallized at temperature T_2 ($\Delta m_{eq}(T_2)$). The crystal yield Y is determined over the 10 min collection time, and the corresponding values are plotted at the different supersaturation levels in Figure 7.
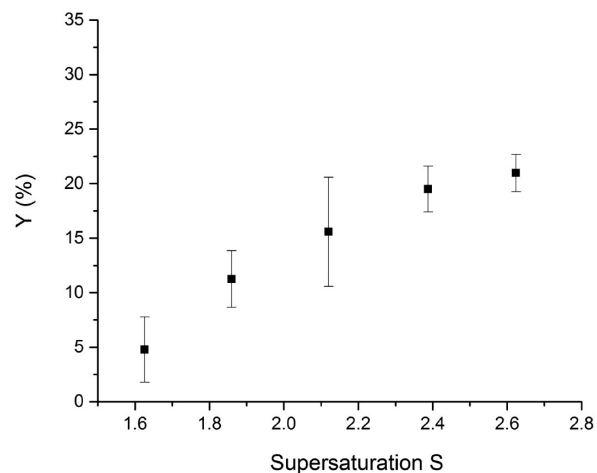

Figure 7. Crystal yield at different supersaturations. Supersaturations investigated: S = 2.62, 2.39, 2.12, 1.86, 1.63, and 1.42. Hexane and adipic acid solution flow rates = 0.3925 mL/min. Sonoprobe tip - capillary external wall distance = 2 mm. Ultrasonic system: Cole-Parmer Instruments 750 W ultrasonic processor, frequency = 20 kHz and amplitude = 21%.

The data show an increase of Y with initial supersaturation. This is explained by the increase of the driving force available for crystallization. Note that only a low percentage (maximum around 20% at the highest supersaturation) of all the available dissolved adipic acid is crystallized. This is probably due to the lack of a growth stage after the sonication stage. In fact, the higher values of yield measured by Narducci et al.[46] for continuous cooling sonocrystallization of adipic acid were obtained with much longer residence times than those used in this work.

4.2. Crystal Morphology. Figure 8 shows pictures of dried (Figure 8a) and resuspended (Figure 8b) adipic acid crystals. In the first figure, agglomerates are observed. Most of these are disrupted in the ultrasound-induced deagglomeration step, which yields smaller groups of crystals or aggregates (Figure 8b). The mean crystal size visible by microscope (ca. 10 μm) is qualitatively in accordance with the mean size $D_{4,3}$ determined by laser diffraction.

In silent conditions, adipic acid normally crystallizes from aqueous solutions as flat, slightly elongated, hexagonal, monoclinic plates[48] (Figure 8c). This characteristic crystalline structure changes when ultrasound is implemented: crystals become more irregular, rounded, and the typical hexagonal-like habit is lost (Figure 8d). The presence of small fragments and the typical irregular geometries observed suggests the occurrence of mechanical disruption induced by cavitation.[16,18]

4.3. Hydrodynamic Effects. Ultrasound is the crucial factor that triggers nucleation at all the supersaturations investigated (Figure 9). The same experiments performed in silent conditions do not show any crystal formation: the droplets appear transparent, and consequently the nucleation rates are practically zero. In Figure 9 the difference between
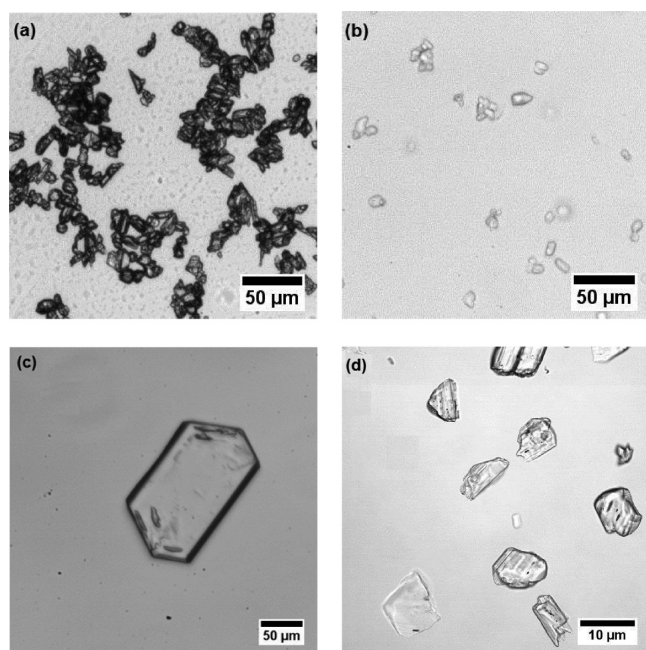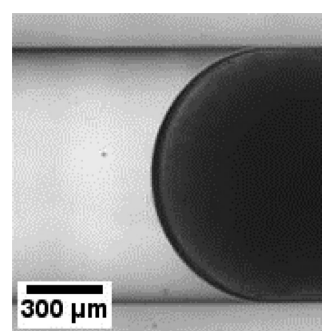
Figure 8. Adipic acid crystals: (a) dried on hot plate, (b) resuspended in vegetable oil, (c) without ultrasound, (d) with ultrasound.

The sonocrystallization event was accompanied by water/hexane emulsification: droplets appeared milky as compared with the clean and transparent droplets without crystals obtained under silent conditions (Figure 9h). Sonoemulsification (SE) and sonocrystallization (SC) were both promoted by sonication. The former occurred at all the supersaturations investigated, as it is not affected by the presence of the crystallizing compound. The latter, on the other hand, is linked to a specific level of supersaturation, as only when a certain supersaturation is reached the crystals are immediately detected. In this regard, the minimum supersaturation ratio at which sonocrystallization was experimentally observed was $S^* = 1.63$ (Figure 9c). For $S < S^*$ crystals were not detected and only sonoemulsification occurred.

For $S < S^*$, an increase of the ultrasonic power, obtained by reducing the sonoprobe tip−capillary distance, did not trigger nucleation: only emulsification was intensified (Figure 10).


Figure 10. Droplet back emulsion, $S = 1.42$, tip-capillary distance = 0.7 mm.

silent and sonicated conditions at all the supersaturation levels is shown. A sharp and marked effect is observed when ultrasound is switched on in terms of immediate crystal production and crystal accumulation at the rear end of the aqueous droplet. This accumulation is most probably induced by the internal droplet mixing which pushes backward the crystals generated by ultrasound.[49] The amount of crystals produced increases with supersaturation in accordance with the yield trend of Figure 7.

To determine if crystals were present within the droplets, we always resorted to visual observation and filtration. No data point is reported for $S < 1.63$, because we could not collect and
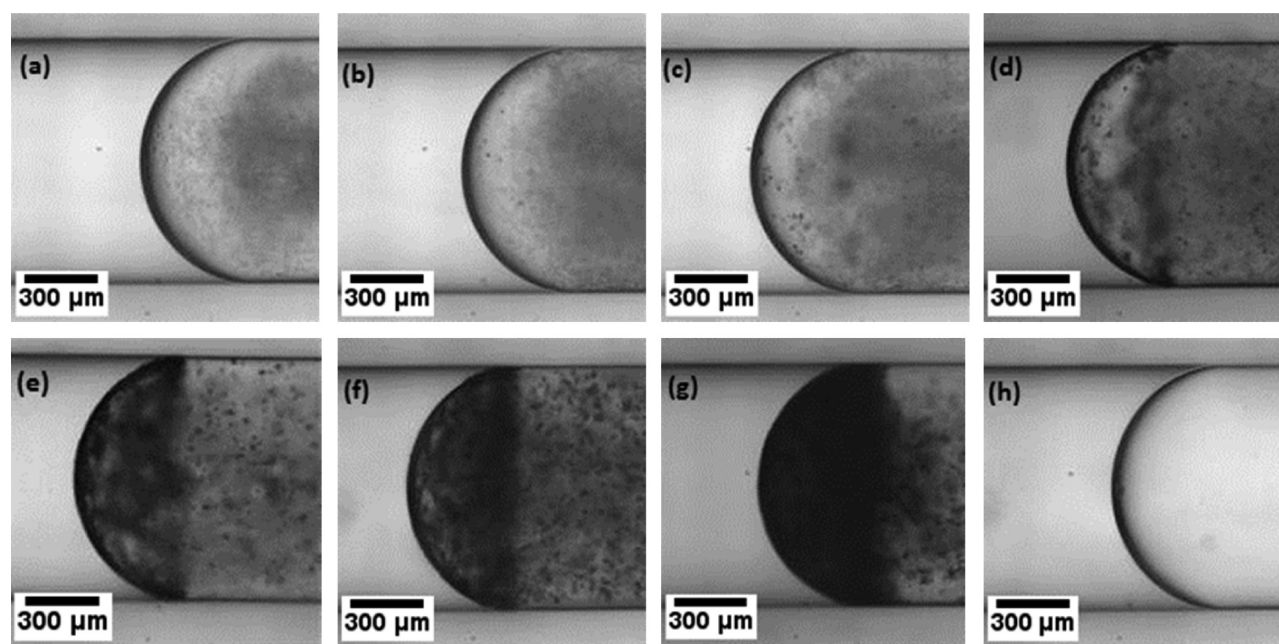
Figure 9. Rear end of aqueous droplets in hexane carrier fluid showing accumulation of crystals at various supersaturation conditions. (a) Without adipic acid, with sonication; (b−g) with adipic acid, with sonication; (h) with adipic acid, without sonication. The flow is from left to right. (b) $S = 1.42$, (c) $S = 1.63$, (d) $S = 1.86$, (e) $S = 2.12$, (f) $S = 2.39$, (g) $S = 2.62$, (h) = 2.62.

Sonoprobe tip-capillary distance
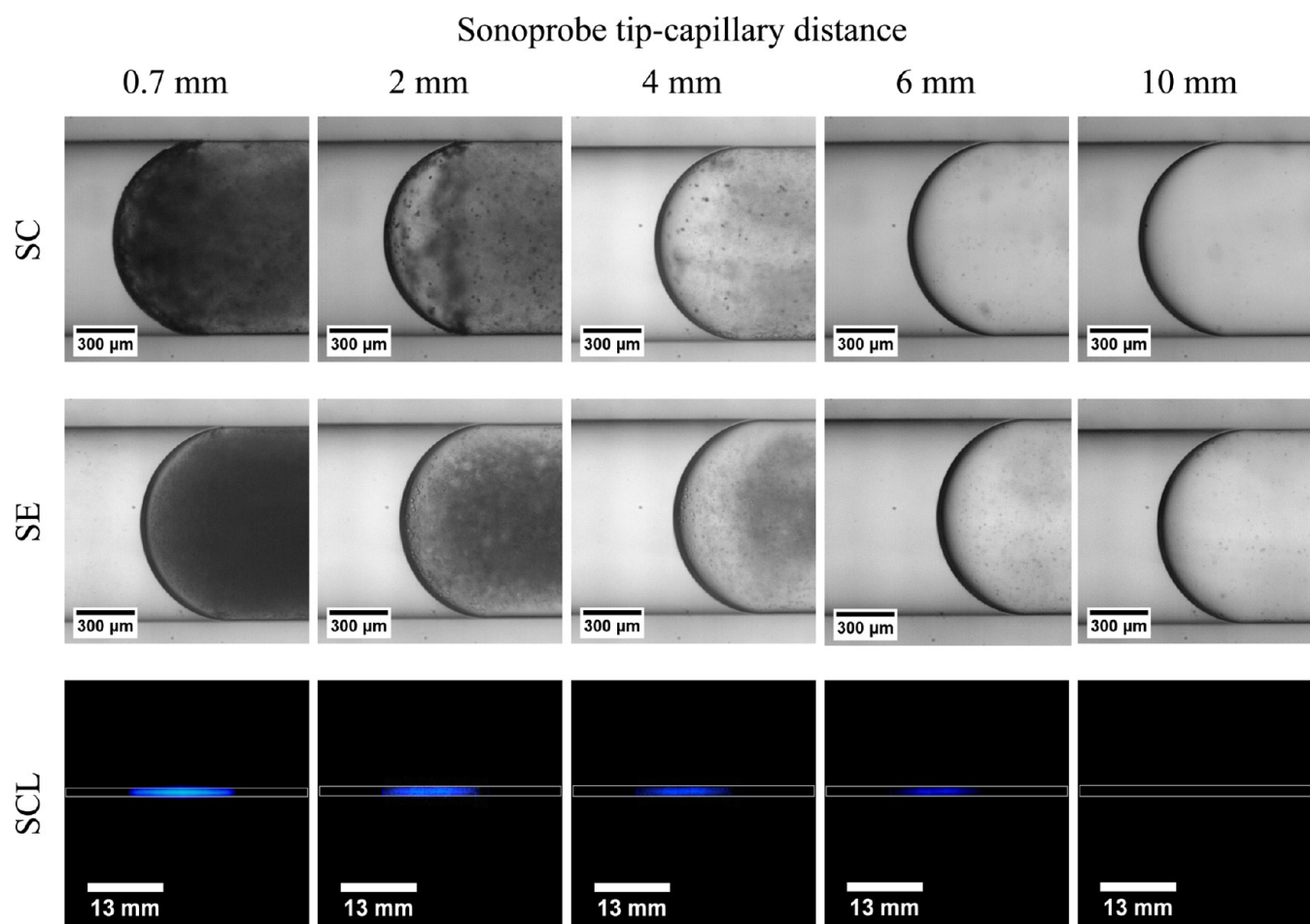
Figure 11. Sonocrystallization (SC), sonoemulsification (SE), and sonochemiluminescence (SCL) at different sonoprobe tip−capillary distances for $S = 1.86$. Luminol solution is flowing within the capillary.

weigh any crystal on the filter paper. This confirms the absence of crystals observed in Figure 9b within the droplets.

4.4. SCL and Its Relation to SE and SC. Above the critical supersaturation level S^*, nucleation is linked to transient cavitation occurring inside the capillary channel, and therefore within the droplet volumes where sonocrystallization takes place. This can be shown by monitoring the direct relation between SCL and SE effects in parallel with the concurring crystal production. For $S > S^*$, as long as the sonoprobe is close to the capillary, we see a direct correspondence between the amount of crystals accumulated at the rear end of the droplet, the intensity of the light emitted by the SCL effect, and the amount of generated emulsion. In Figure 11, the relation among the three phenomena for a supersaturation of $S = 1.86$ is examined. Similar trends were observed for all the supersaturations investigated. In all cases, above a sonoprobe tip−capillary distance of 10 mm, SCL, SE, and SC were not detectable. In conclusion, as transient cavitation is required for both SCL and SE,[28] the results indicate that transient cavitation is crucial for sonocrystallization.

Figure 12 provides qualitative indication of transient cavitation occurring below the sonoprobe tip surface. If the capillary is removed and the luminol solution is placed directly within the Perspex enclosure, a cone-shaped bright area is observed. The sonochemiluminescence detected is the consequence of the cavitation bubbles self-arranged in the typical cone-like macrostructure in the vicinity of the
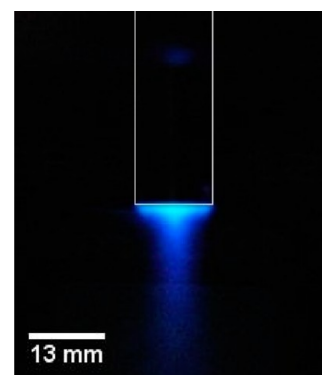
Figure 12. Sonochemiluminescence below the sonoprobe tip. A luminol solution is placed within the Perspex enclosure and the capillary is removed.

sonoprobe tip flat surface.[50] A consistent attenuation of the light intensity and consequently of transient cavitation is registered after approximately 10 mm. This is in accordance with Figure 11. After a distance of 10 mm, the acoustic pressure decreases to a level at which cavitation is less likely to occur, and therefore SCL, SC, and SE are drastically reduced (for more details, see section 4.5). In this regard, we should note that the plastic capillary is acoustically transparent, so that the acoustic field is not affected by its presence.
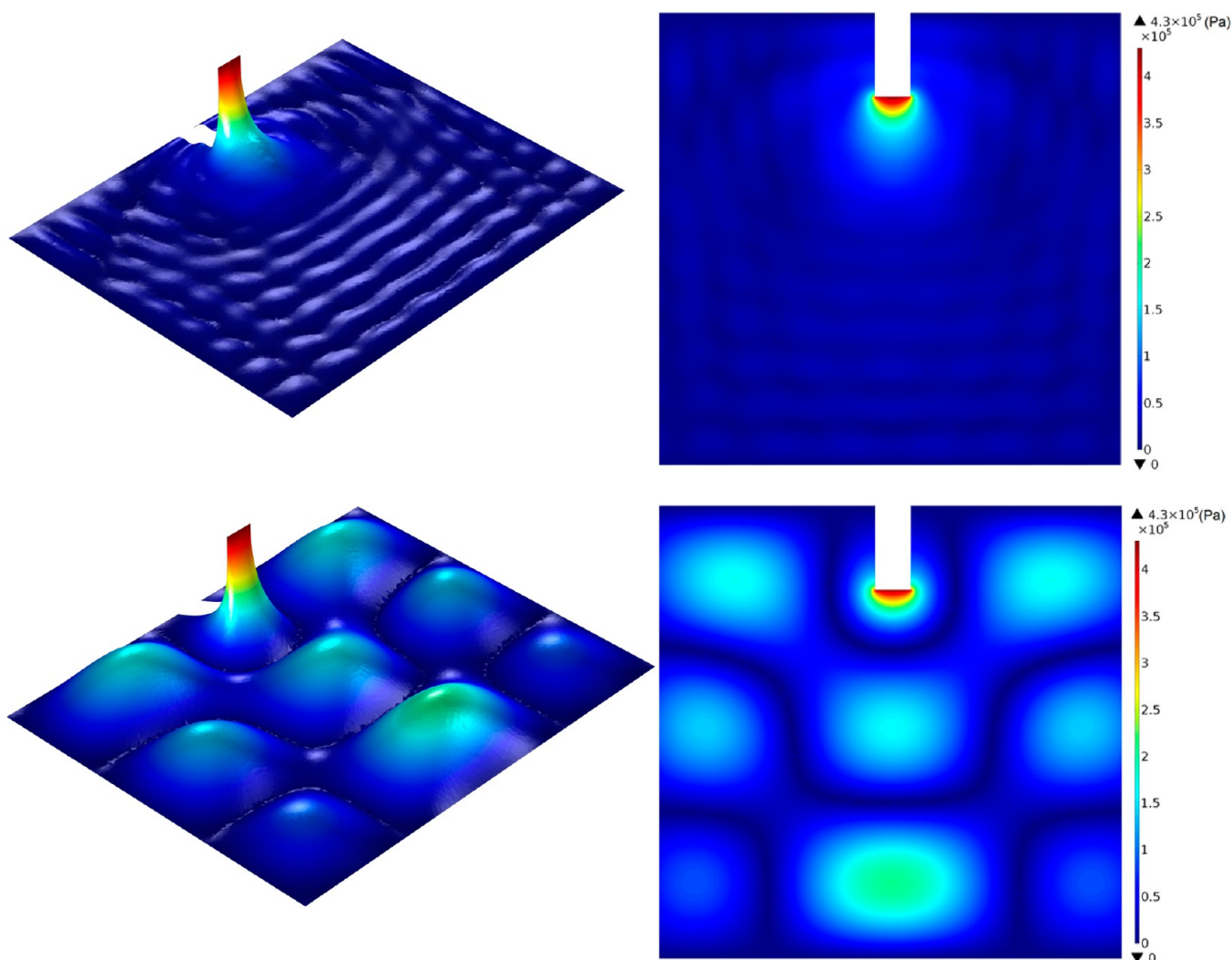
Figure 13. Acoustic pressure distribution on a cutting plane passing through the middle cross section of the sonoprobe. Top: with, bottom: without damping effect of bubbles.

4.5. Cavitation Analysis Using the Results of the Numerical Simulation. Numerical results for distribution of the pressure amplitude on a cross section passing through the middle of the sonoprobe are shown in Figure 13. To illustrate the sensitivity of the model to the attenuation of the wave due to the bubbles, the Helmholtz equation was also solved for a case without the damping term. The corresponding results are also shown in Figure 13 for comparison. It can be seen that the damping effect of the bubbles has a significant influence on the distribution of the pressure amplitude. Therefore, it is important to consider the attenuation effect when simulation and design of sonocrystallizers are of interest.

The pressure drops away from the tip due to the absorbing behavior of the side walls as well as damping effect of the bubbles. It is concluded that, if the consequences of higher acoustic pressure, such as transient cavitation, are desirable, the distance between the sonoprobe and the capillary carrying the solution should be kept to a minimum.

To quantify this conclusion, the radial dynamics of bubbles are modeled at different pressure amplitudes descending from 4.3×10^5 Pa, which is the amplitude at the surface of the sonoprobe. The results are shown in Figure 14. If the bubble experiences a violent collapse, the Mach number exceeds one
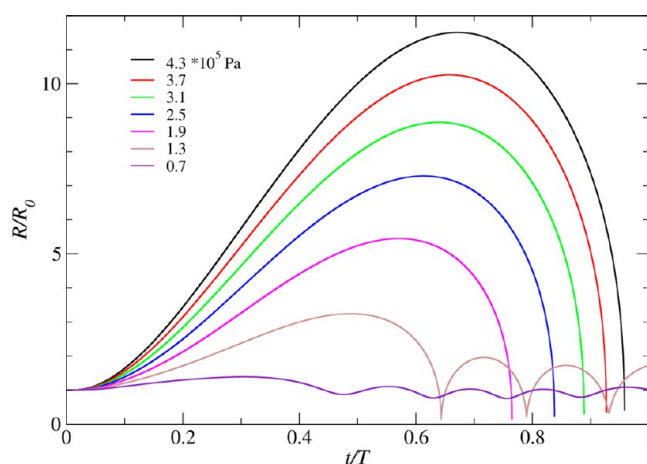
Figure 14. Bubble radial dynamics over one acoustic cycle for a bubble with $R_0 = 30$ μm at different pressure amplitudes.

and the program stops computing the radial dynamics. This trend can be seen in the figure for pressure amplitudes higher than and equal to 1.9×10^5 Pa. For amplitudes below this value the bubbles tend to oscillate nonlinearly. Although it is difficult

to define a sharp threshold, the value of 1.9×10^5 Pa can be used as an approximate threshold for transient cavitation in this case. Hence, the zone near the sonoprobe where we expect the bubbles to experience transient cavitation could be predicted from the simulation. This is illustrated in Figure 15 in which the
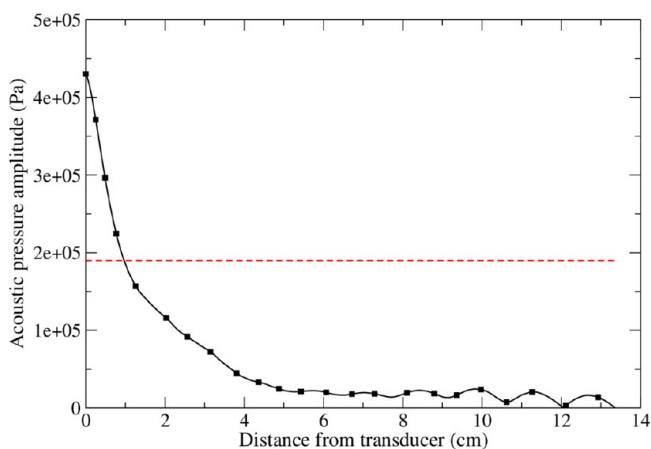
Figure 15. Pressure amplitude along the axis of the sonoprobe to the bottom of the reactor. The horizontal dashed line shows the transient cavitation threshold.

decreasing pressure amplitude is plotted versus the distance along the axis of the horn. For comparison, the transient cavitation threshold is shown in the graph as the horizontal dashed line. According to the figure, pressure drops in approximately 1 cm from the tip to values below the threshold. This is in agreement with the experimental results in which no crystals and no SCL were observed after increasing the distance between the capillary and the sonoprobe beyond 1 cm. For more reliable predictions of cavitation activity and correlating it to nucleation of crystals, we propose to measure the initial distribution of bubbles and their void fraction in a more precise way, because they do affect the pressure distribution, as it is depicted in this work.

5. CONCLUSIONS

In this work, a new microfluidic continuous device for production of adipic acid crystals is presented. The system is able to provide crystals with a very small mean size at high production rates. The crystal size distributions and the corresponding mean size of crystals remain the same by changing the supersaturation level. However, the production rate (crystal yield) increases by increasing the supersaturation. Besides that, studying cavitation using sonochemiluminesence and sonoemulsification experiments reveal that after a distance of about 1 cm from the sonoprobe tip, all of the consequences of cavitation disappear. This observation is investigated numerically by simulation of the wave propagation in the medium. Numerical results show that the attenuating effect of cavitation bubbles should be considered since it has a significant effect in predicting the pressure amplitude inside the sonocrystallizer. By assuming a reasonable initial bubble nuclei size and void fraction, this effect is implemented in the simulation. Moreover, an acoustical Mach number above one is set as the threshold for transient cavitation. The analysis shows that the expected zones for transient cavitation are predictable by numerical simulations. Furthermore, it is concluded that transient cavitation of bubbles and its consequences are a

significant mechanism for enhancing nucleation of crystals among several proposed in the literature.

■ AUTHOR INFORMATION

Corresponding Author
*E-mail: l.mazzei@ucl.ac.uk.

Notes
The authors declare no competing financial interest.

■ REFERENCES

(1) Variankaval, N.; Cote, A. S.; Doherty, M. F. From Form to Function: Crystallization of Active Pharmaceutical Ingredients. *AIChE J.* **2008**, *54*, 1682−1688.

(2) Mullin, J. W. *Crystallization*; Butterworth-Heinemann: Oxford, 2001.

(3) Dittrich, P. S.; Manz, A. Lab-on-a-chip: microfluidics in drug discovery. *Nat. Rev. Drug Discovery* **2006**, *5*, 210−8.

(4) Elvira, K. S.; Casadevall i Solvas, X.; Wootton, R. C. R.; de Mello, A. J. The past, present and potential for microfluidic reactor technology in chemical synthesis. *Nat. Chem.* **2013**, *5*, 905−915.

(5) Ildefonso, M.; Candoni, N.; Veesler, S. Using Microfluidics for Fast, Accurate Measurement of Lysozyme Nucleation Kinetics. *Cryst. Growth Des.* **2011**, *11*, 1527−1530.

(6) Marre, S.; Jensen, K. F. Synthesis of micro and nanostructures in microfluidic systems. *Chem. Soc. Rev.* **2010**, *39*, 1183−202.

(7) Poe, S. L.; Cummings, M. a; Haaf, M. P.; McQuade, D. T. Solving the clogging problem: precipitate-forming reactions in flow. *Angew. Chem., Int. Ed.* **2006**, *45*, 1544−8.

(8) Eder, R. J. P.; Radl, S.; Schmitt, E.; Innerhofer, S.; Maier, M.; Gruber-Woelfler, H.; Khinast, J. G. Continuously seeded, continuously operated tubular crystallizer for the production of active pharmaceutical ingredients. *Cryst. Growth Des.* **2010**, *10*, 2247−2257.

(9) Besenhard, M. O.; Hohl, R.; Hodzic, A.; Eder, R. J. P.; Khinast, J. G. Modeling a seeded continuous crystallizer for the production of active pharmaceutical ingredients. *Cryst. Res. Technol.* **2014**, *49*, 92−108.

(10) Suslick, K. S. Sonochemistry. In *Kirk-Othmer Encyclopedia of Chemical Tecnology*; Kirk, R. E.; Othmer, D. F.; Kroschwitz, J. I.; Howe-Grant, M. John Wiley & Sons: New York, 1998

(11) Mason, T. J. Ultrasound in synthetic organic chemistry. *Chem. Soc. Rev.* **1997**, *26*, 443−451.

(12) Cains, P. W.; Martin, P. D.; Price, C. J. The Use of Ultrasound in Industrial Chemical Synthesis and Crystallization. 1. Applications to Synthetic Chemistry . *Org. Process Res. Dev.* **1998**, *2*, 34−48.

(13) Hem, S. L. The effect of ultrasonic vibrations on crystallization processes. *Ultrasonics* **1967**, *5*, 202−207.

(14) Virone, C.; Kramer, H. J. M.; van Rosmalen, G. M.; Stoop, A. H.; Bakker, T. W. Primary nucleation induced by ultrasonic cavitation. *J. Cryst. Growth* **2006**, *294*, 9−15.

(15) Harzali, H.; Baillon, F.; Louisnard, O.; Espitalier, F.; Mgaidi, a. Experimental study of sono-crystallisation of ZnSO4·7H2O, and interpretation by the segregation theory. *Ultrason. Sonochem.* **2011**, *18*, 1097−106.

(16) Ruecroft, G.; Hipkiss, D.; Ly, T.; Maxted, N.; Cains, P. W. Sonocrystallization: The use of ultrasound for improved industrial crystallization. *Org. Process Res. Dev.* **2005**, *9*, 923−932.

(17) McCausland, L. J.; Cains, P. W.; Martin, P. D. Use the Power of Sonocrystallization for Improved Properties. *Chem. Eng. Prog.* **2001**, 56−61.

(18) Luque de Castro, M. D.; Priego-Capote, F. Ultrasound-assisted crystallization (sonocrystallization). *Ultrason. Sonochem.* **2007**, *14*, 717−24.

(19) Miyasaka, E.; Kato, Y.; Hagisawa, M.; Hirasawa, I. Effect of ultrasonic irradiation on the number of acetylsalicylic acid crystals produced under the supersaturated condition and the ability of controlling the final crystal size via primary nucleation. *J. Cryst. Growth* **2006**, *289*, 324−330.

(20) Lyczko, N.; Espitalier, F.; Louisnard, O.; Schwartzentruber, J. Effect of ultrasound on the induction time and the metastable zone widths of potassium sulphate. *Chem. Eng. J.* 2002, *86*, 233−241.

(21) Kordylla, A.; Koch, S.; Tumakaka, F.; Schembecker, G. Towards an optimized crystallization with ultrasound: Effect of solvent properties and ultrasonic process parameters. *J. Cryst. Growth* 2008, *310*, 4177−4184.

(22) Jiang, M.; Papageorgiou, C. D.; Waetzig, J.; Hardy, A.; Langston, M.; Braatz, R. D. Indirect Ultrasonication in Continuous Slug-Flow Crystallization. *Cryst. Growth Des.* 2015, *15*, 2486−2492.

(23) Benzinger, W.; Schygulla, U.; Jäger, M.; Schubert, K. Anti fouling investigations with ultrasound in a microstructured heat exchanger. In *ECI Symposium Series, Proceedings of 6th International Conference on Heat Exchanger Fouling and Cleaning - Challenges and Opportunities*; Müller-Steinhagen, H., Reza Malayeri, M., Watkinson, A. Paul, Eds.; June 5−10, 2005.

(24) Flowers, B. S.; Hartman, R. L. Particle Handling Techniques in Microchemical Processes. *Challenges* 2012, *3*, 194−211.

(25) Hartman, R. L. Managing Solids in Microreactors for the Upstream Continuous Processing of Fine Chemicals. *Org. Process Res. Dev.* 2012, *16*, 870−887.

(26) Wu, K.; Kuhn, S. Strategies for solids handling in microreactors. *Chim. Oggi/Chem. Today* 2014, *32*, 62−66.

(27) Eder, R. J. P.; Schrank, S.; Besenhard, M. O.; Roblegg, E.; Gruber-Woelfler, H.; Khinast, J. G. Continuous Sonocrystallization of Acetylsalicylic Acid (ASA): Control of Crystal Size. *Cryst. Growth Des.* 2012, *12*, 4733−4738.

(28) Cucheval, A.; Chow, R. C. Y. A study on the emulsification of oil by power ultrasound. *Ultrason. Sonochem.* 2008, *15*, 916−20.

(29) Ashokkumar, M.; Lee, J.; Iida, Y.; Yasui, K.; Kozuka, T.; Tuziuti, T.; Towata, A. Spatial distribution of acoustic cavitation bubbles at different ultrasound frequencies. *ChemPhysChem* 2010, *11*, 1680−4.

(30) Rossi, D.; Gavriilidis, A.; Kuhn, S.; Candel, M. A.; Jones, A. G.; Price, C.; Mazzei, L. Adipic Acid Primary Nucleation Kinetics from Probability Distributions in Droplet-Based Systems under Stagnant and Flow Conditions. *Cryst. Growth Des.* 2015, *15*, 1784−1791.

(31) Stojanovic, Z. Determination of particle size distributions by laser diffraction. *Technol. - New Mater. 21*, (2012).

(32) Henglein, A.; Ulrich, R.; Lilie, J. Luminescence and Chemical Action by Pulsed Ultrasound. *J. Am. Chem. Soc.* 1989, *111*, 1974−1979.

(33) Tandiono; Ohl, S. W.; Ow, D. S. W.; Klaseboer, E.; Wong, V. V.; Dumke, R.; Ohl, C. D. Sonochemistry and sonoluminescence in microfluidics. *Proc. Natl. Acad. Sci. U. S. A.* 2011, *108*, 5996−5998.

(34) Fernandez Rivas, D.; Ashokkumar, M.; Leong, T.; Yasui, K.; Tuziuti, T.; Kentish, S.; Lohse, D.; Gardeniers, H. J. G. E. Sonoluminescence and sonochemiluminescence from a microreactor. *Ultrason. Sonochem.* 2012, *19*, 1252−1259.

(35) Rooze, J.; Rebrov, E. V.; Schouten, J. C.; Keurentjes, J. T. F. Effect of resonance frequency, power input, and saturation gas type on the oxidation efficiency of an ultrasound horn. *Ultrason. Sonochem.* 2011, *18*, 209−15.

(36) Commander, K. W. Linear pressure waves in bubbly liquids: Comparison between theory and experiments. *J. Acoust. Soc. Am.* 1989, *85*, 732.

(37) Labouret, S.; Frohly, J. Bubble size distribution estimation via void rate dissipation in gas saturated liquid. Application to ultrasonic cavitation bubble fields. *Eur. Phys. J.: Appl. Phys.* 2002, *19*, 39−54.

(38) Rozenberg, L. D. *High-Intensity Ultrasonic Fields*; Springer: Berlin, 1971.

(39) Dähnke, S.; Keil, F. Modeling of Three-Dimensional Linear Pressure Fields in sonochemical reactors with homogeneous and inhomogeneous Density Distributions of Cavitation Bubbles. *Ind. Eng. Chem. Res.* 1998, *37*, 848−864.

(40) Sutkar, V. S.; Gogate, P. R.; Csoka, L. Theoretical prediction of cavitational activity distribution in sonochemical reactors. *Chem. Eng. J.* 2010, *158*, 290−295.

(41) Jamshidi, R.; Pohl, B.; Peuker, U. a.; Brenner, G. Numerical investigation of sonochemical reactors considering the effect of inhomogeneous bubble clouds on ultrasonic wave propagation. *Chem. Eng. J.* 2012, *189−190*, 364−375.

(42) Raman, V.; Abbas, A.; Joshi, S. C. Mapping Local Cavitation Events in High Intensity Ultrasound (HIU) fields. *Chem. Eng.* 2006, 1−19.

(43) Klíma, J.; Frias-Ferrer, A.; González-García, J.; Ludvík, J.; Sáez, V.; Iniesta, J. Optimisation of 20 kHz sonoreactor geometry on the basis of numerical simulation of local ultrasonic intensity and qualitative comparison with experimental results. *Ultrason. Sonochem.* 2007, *14*, 19−28.

(44) Lauterborn, W. Numerical investigation of nonlinear oscillations of gas bubbles in liquids. *J. Acoust. Soc. Am.* 1976, *59*, 283.

(45) Keller, J. B. Bubble oscillations of large amplitude. *J. Acoust. Soc. Am.* 1980, *68*, 628.

(46) Narducci, O.; Jones, a. G.; Kougoulos, E. Continuous crystallization of adipic acid with ultrasound. *Chem. Eng. Sci.* 2011, *66*, 1069−1076.

(47) Narducci, O.; Jones, A. G.; Kougoulos, E. *Cryst. Growth Des.* 2011, *11*, 1742−1749.

(48) Clydesdale, G.; Thomson, G. B.; Walker, E. M.; Roberts, K. J.; Meenan, P.; Docherty, R. A Molecular Modeling Study of the Crystal Morphology of Adipic Acid and Its Habit Modification by Homologous. *Cryst. Growth Des.* 2005, *5*, 2154−2163.

(49) Dore, V.; Tsaoulidis, D.; Angeli, P. Mixing patterns in water plugs during water/ionic liquid segmented flow in microchannels. *Chem. Eng. Sci.* 2012, *80*, 334−341.

(50) Moussatov, A.; Granger, C.; Dubus, B. Cone-like bubble formation in ultrasonic cavitation field. *Ultrason. Sonochem.* 2003, *10*, 191−195.